

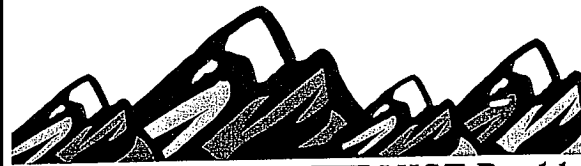
**2008 Conference on  
Precision Electromagnetic  
Measurements**

**Digest**

**8-13 June 2008**

**Broomfield, Colorado**

**CPEM 2008**



**NIST Boulder**

# ANTENNA TEST RANGE IMAGING USING SPHERICAL NEAR-FIELD SCANNING

M. H. Francis, R. C. Wittmann, and R. H. Direen  
National Institute of Standards and Technology  
Broadway, Mailstop, Boulder, CO, USA

## Abstract

Although the theory is straightforward, practical implementation of spherical near-field scanning for evaluating test chambers presents some significant challenges. Among these are the selection of an appropriate probe and the difficulty in minimizing support-structure blockage. We report on recent NIST efforts to address these difficulties and present our most recent results.

## Introduction

We discuss recent measurements performed at the National Institute of Standards and Technology (NIST) that were used to characterize the incident fields within a test volume and to produce images of the test chamber. The probe (Figure 1), on a roll-over-azimuth mount, was scanned over a spherical surface enclosing the test volume. A ladder with a small metal plate (Figure 2) and a bicycle (Figure 1) were both included in the scene. Illumination was alternately provided by standard gain horns mounted on the wall and on a tripod (Figure 3) in the first measurement setup and a cassegrain dish mounted on the wall and a circular waveguide on a tripod in setup 2. In setup 1, we used a probe with a gain of about 7 dB, while in setup 2 we used a probe with a gain of about 22 dB.

The origin of the laboratory coordinate system is the center of the measurement sphere, the  $x$  axis is directed (horizontally) from this origin through the middle of the wall horn aperture, and the  $z$  axis is directed upward. Polar angles  $\theta$  and  $\phi$  are defined in the usual manner. When  $\theta = 0^\circ$  the probe points toward the ceiling; when  $\theta = 90^\circ$  and  $\phi = 0^\circ$ , the probe points toward the wall horn; and when  $\theta = 90^\circ$  and  $\phi = 90^\circ$ , the probe points in the  $y$  direction. This coordinate system is used in the collection, analysis, and presentation of the data.

Measurements were made at 16 GHz; the measurement sphere radius was  $r_p = 64$  cm (in measurement 1) and  $r_p = 75$  cm (in measurement 2). The data were collected at  $0.75^\circ$  increments in  $\theta$  and  $\phi$  in measurement 1 and  $0.75^\circ$  increments in measurement 2.

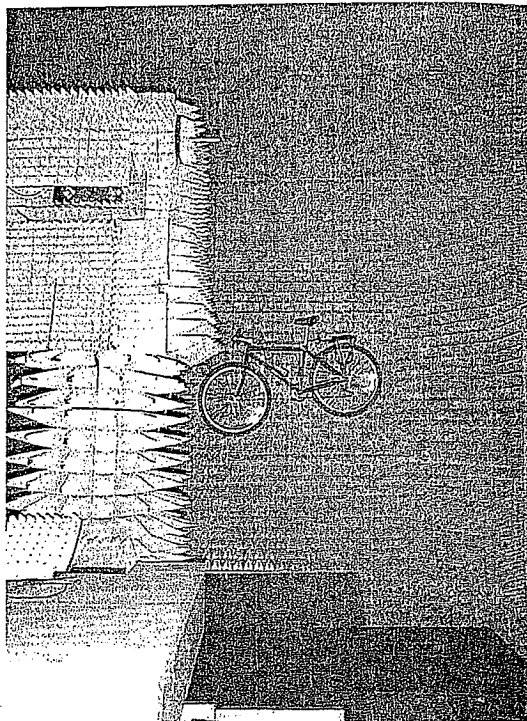


Figure 1: Probe (top center) and bicycle

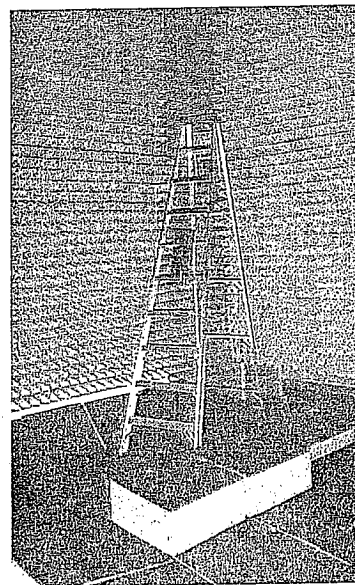


Figure 2: Ladder and plate

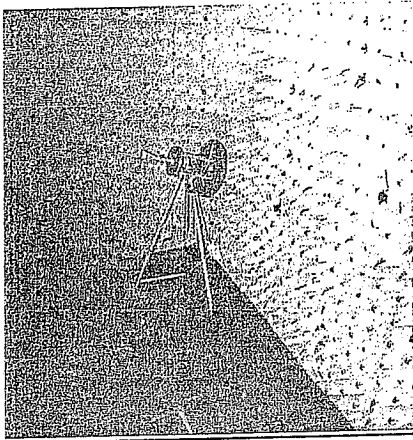


Figure 3: Tripod horn

### Theory

The technique is based on a plane-wave representation of the incident field

$$\mathbf{E}_i(\mathbf{r}) = \frac{1}{4\pi} \int \mathbf{a}_N(\hat{\mathbf{k}}) \exp(i\mathbf{k} \cdot \mathbf{r}) d\hat{\mathbf{k}} \quad (1)$$

$$\mathbf{a}_N(\hat{\mathbf{r}}) = \sum_{n=1}^N \sum_{m=-n}^n [a_{nm}^1 \mathbf{X}_{nm}(\hat{\mathbf{r}}) + a_{nm}^2 \mathbf{Y}_{nm}(\hat{\mathbf{r}})], \quad (2)$$

where the integral is over  $4\pi$ ,  $k = |\mathbf{k}| = 2\pi/\lambda$ , and  $\mathbf{X}_{nm}$  and  $\mathbf{Y}_{nm}$  are vector spherical harmonics [1, chp. 16]. Here,  $N \sim kr_p$ . The algorithm described in [2] allows calculation of the coefficients  $a_{nm}^1$  and  $a_{nm}^2$  from the measured data. Once these coefficients are known, then (1) can be used to determine the field anywhere inside the test volume. The theory accounts for probe pattern effects.

An image can be formed by simply plotting  $|\mathbf{a}_N|$ . For example, it is apparent from (1) that the image of the plane wave  $\mathbf{E}_0 \exp(i\mathbf{k}_0 \cdot \mathbf{r})$  must be proportional to  $|\delta_N(\hat{\mathbf{r}} - \hat{\mathbf{k}}_0)|$  where  $\delta_N$  approaches the Dirac delta function as  $N \rightarrow \infty$ . The angular resolution (Rayleigh criterion) is inversely proportional to  $N$  [2].

### Images

In Figures 4, the tripod horn is the source of radiation. Figure 4 is focused on the bicycle. The bicycle is clearly recognizable along with some structural detail. The ladder, however, is only weakly illuminated. In particular the attached metal plate is not obvious, presumably because the specular reflection is not directed through the measurement sphere. (In Figure 4,  $\theta$  varies from  $-90^\circ$  to  $90^\circ$  vertically and  $\phi$  varies from  $180^\circ$  to  $-180^\circ$  horizontally. The lower left corner corresponds to  $\theta = -90^\circ$ ,  $\phi = 180^\circ$ .)

In an effort to improve the effective dynamic range, measurement 2 was done with a higher gain probe. We will report on the results at the conference

Although the emphasis of this presentation is on imaging results, we note that it is possible to determine the best-fit plane wave to the incident field  $\mathbf{E}_i(\mathbf{r})$  and the departure of the incident field from the best-fit plane wave. This allows us to characterize the quality of a compact range test zone.

### References

- [1] J. D. Jackson, *Classical Electrodynamics*, 2nd edition. New York, Wiley, 1975.
- [2] R. C. Wittmann, "Spherical near-field scanning: Determining the incident field near a rotatable probe," *1990 IEEE Antennas and Propagation Symposium Digest*, pp. 224-227, May 7-11, 1990.
- [3] R. C. Wittmann, and D. N. Black, "Antenna/RCS range evaluation using a spherical synthetic aperture radar," *Proc. AMTA*, Seattle, pp.406-410, Sept. 30-Oct. 3, 1996.
- [4] R. C. Wittmann, and M. H. Francis, "Antenna Range Imaging," *Proc. AMTA*, Philadelphia, pp.234-236, Oct. 16-20, 2000.
- [5] R. C. Wittmann, B. K. Alpert, and M. H. Francis, "Near-field antenna measurements using nonideal measurement locations," *IEEE Trans. Antennas Propagat.*, vol. AP-46, pp. 716-722, May 1998.

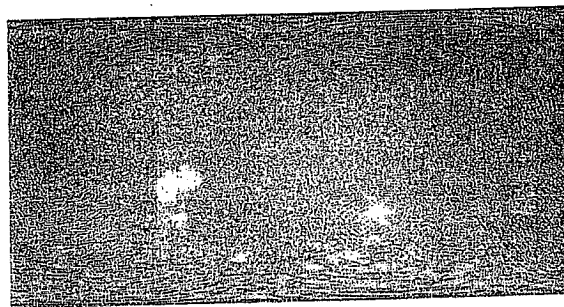


Figure 4: Image focused on bicycle